Dalton Transactions

PAPER

View Article Online
View Journal

Cite this: DOI: 10.1039/c6dt03200a

Metallohydrolase biomimetics with catalytic and structural flexibility†

Luisa L. Mendes,[a] Daniel Englert,[b] Christiane Fernandes,[a] Lawrence R. Gahan,[c] Gerhard Schenk*[c] and Adolfo Horn, Jr.*[a]

Received 11th August 2016,
Accepted 26th September 2016

DOI: 10.1039/c6dt03200a

www.rsc.org/dalton

The structural and functional properties of zinc(II) complexes of two nitrogen rich polydentate ligands, HTPDP = 1,3-bis(bis-pyridin-2-ylmethylamino)propan-2-ol and HTPPNOL = *N*,*N*,*N*′-tris-(2-pyridylmethyl)-1,3-diaminopropan-2-ol, are compared. HTPDP is a hepta-dentate ligand with four pyridyl groups attached to a 1,3-diaminopropan-2-ol backbone while HTPPNOL contains only three pyridyl groups. In reactions with $Zn(ClO_4)_2$, HTPDP forms a dinuclear zinc compound $[Zn_2(TPDP)(OAc)](ClO_4)_2$, **1**. On the other hand, mononuclear $[Zn(HTPPNOL)](ClO_4)_2$, **2**, and tetranuclear $[Zn_4(TPPNOL)_2(OAc)_3](ClO_4)_3$, **3**, complexes were isolated with the ligand HTPPNOL. Kinetic measurements with the substrate bis(2,4-dinitrophenyl)phosphate (BDNPP) revealed that compound **1** (k_{cat} = 31.4 × 10^{-3} min^{-1}) is more reactive than **3** (k_{cat} = 7.7 × 10^{-3} min^{-1}) at pH = 8.5, whilst the mononuclear compound **2** is inactive. Compound **1** displays a typical steady-state kinetic behaviour, while compound **3** exhibits steady-state behaviour only ~120 s after starting the reaction, preceded by a burst-phase. ^{31}P NMR studies confirm that **1** can promote the hydrolysis of both ester bonds in BDNPP, generating the monoester DNPP and inorganic phosphate in the process. In contrast, DNPP is not a substrate for **3**. The crystal structure of the complex formed by **3** and DNPP reveals the formation of a tetranuclear zinc complex $[Zn_4(TPPNOL)_2(DNPP)_2](ClO_4)_2$, **4**, in which the phosphate moiety of DNPP adopts an unusual tridentate μ–η^1:η^1:η^1 coordination mode.

Introduction

Metallohydrolases are a large and diverse family of enzymes that cover a broad range of metabolic functions, including DNA proofreading, biosynthesis of a range of biomolecules, and also the control of neurological functions.[1,2] Some of these enzymes recently evolved specific activities to address environmental and medical challenges such as the increased use of pesticides and antibiotics.[3–5] Whilst carboxypeptidase A[6,7] and thermolysin[8–10] are examples of mononuclear metallohydrolases most metallohydrolases require a set of two identical divalent ions like zinc(II), nickel(II) or manganese(II).[11–14] An exception are purple acid phosphatases (PAPs), which possess a heterovalent binuclear centre with an iron(III) and a second divalent metal ion, generally a zinc(II) or manganese(II) for plant enzymes and a redox-active iron for their mammalian counterparts.[15–17] Metallophosphatases such as PAPs have received considerable attention not only due to their mechanistic diversity but also due to the broad spectrum of substrates they are capable of hydrolyzing. Such enzymes have been shown to act on not only mono, di- and tri-phosphate esters, including natural substrates such as carbohydrates, peptides, DNA and RNA, but also on synthetic compounds such as pesticides and nerve gases.[4,18–27]

The development of synthetic analogs for such metallophosphatases has provided useful benchmarks to address questions about the structure and mechanism of such enzymes.[1,28,29] Furthermore, such compounds also hold significant potential for various applications, including as chemotherapeutics in anticancer treatments[30–32] or catalysts for the degradation of toxic organophosphates.[4,26,33,34] One of the most successful families of ligands employed in the synthesis of metallophosphatase models has been built on the 2,6-bis(aminomethyl)-4-methylphenol backbone, which may provide as many as seven ligands for the coordination environments of the two metal ions, and in which a cresol unit acts as the metal-bridging group.[35,36] Both symmetric and non-symmetric

[a]*Laboratório de Ciências Químicas, Universidade Estadual do Norte Fluminense, 28013-602 Campos dos Goytacazes/RJ, Brazil. E-mail: adolfo@uenf.br; Fax: +55 22 2739 7046; Tel: +55 22 2739 7384*

[b]*Anorganisch-Chemisches Institut, Universität Heidelberg, Im Neuenheimer Feld 270, 69120 Heidelberg, Germany*

[c]*School of Chemistry and Molecular Biosciences, The University of Queensland, Brisbane, QLD 4072, Australia. E-mail: schenk@uq.edu.au; Fax: +61 7 3365 4273; Tel: +61 7 3365 4144*

† Electronic supplementary information (ESI) available. CCDC 1495702–1495704. For ESI and crystallographic data in CIF or other electronic format see DOI: 10.1039/c6dt03200a

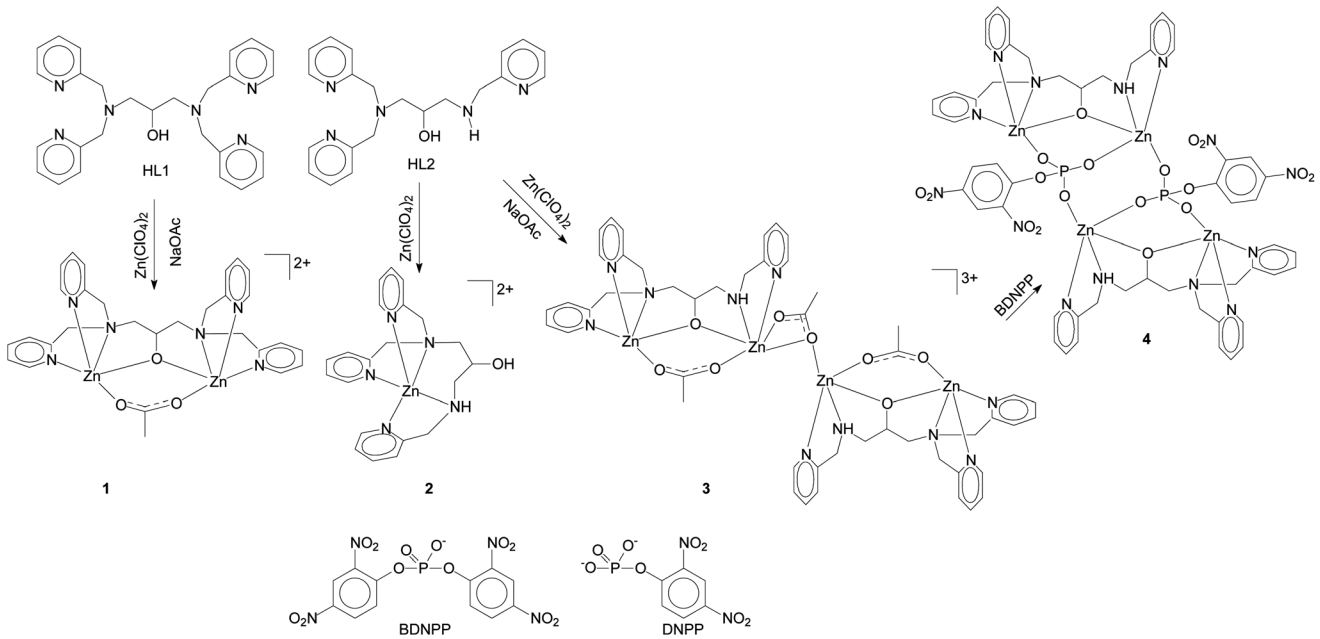

Fig. 1 Scheme showing the structure of the ligands and complexes prepared in this work and the phosphate esters BDNPP and DNPP as well.

examples have been described.[37–42] Features such as substituent effects,[43] bridging groups[32,36,44,45] and, more recently, the effect of the second coordination sphere have been evaluated for their influence on the catalytic performance of such biomimetics.[44,46–48] Depending on the metal ion employed in the synthesis, the addition of carboxylate groups (*e.g.* acetate, benzoate) to the reaction mixture may result in five- or six-coordinated metal ions. In an aqueous environment such carboxylate ligands may be displaced by water molecules, resulting in the coordination of water molecules to the metal ions, which, at suitable pH values, may form hydroxo species that play an essential role in the reactivity of these biomimetics.[49–57] Another dinucleating unit that has been employed in the synthesis of metallophosphatase models is the 1,3-diamino-2-hydroxypropane molecule,[58,59] which also provides up to seven metal-coordinating ligands, and with a deprotonated alcohol group acting frequently as a metal-bridging unit. For this ligand system symmetric compounds are easily synthesized, but their non-symmetric counterparts require more elaborate synthetic pathways.[60,61] This may also be one of the main reasons why the majority of synthetic models for phosphatase use aromatic rather than aliphatic bridging ligands.

Although the effects of the substituent on the aromatic rings and the importance of the hydrogen donor groups for the catalytic reaction have been described, a point that has been scarcely addressed is related to the presence of an additional vacant site in the first coordination sphere of the dinuclear metal centre, mainly present with ligands that contain the 1,3-diamino-2-hydroxypropane unit. Specifically, the effect of an additional vacancy in the coordination environment on the catalytic proficiency of such biomimetics is largely unknown. Here, we address this question by comparing the properties of zinc(II) complexes generated with either a hepta- (HL1) or hexa- (HL2) dentate ligand (Fig. 1).

Experimental

General methods

^{1}H and ^{13}C NMR (see the ESI†) spectra were recorded with a 300, 400 or 500 MHz Bruker Advance Spectrometer. Data processing was carried out with TOPSPIN from Bruker. Chemical shifts of the final ligands were assigned using two-dimensional correlation spectroscopy (COSY), heterodinuclear single quantum correlation (HSQC), heterodinuclear multiple bond connectivity (HMBC) and distortionless enhancement by polarization transfer (DEPT). Infrared spectra were recorded using a PerkinElmer FT-IR/NIR Frontier Spectrometer with a diamond/ZnSe crystal, using a Universal ATR Sampling Accessory. Elemental analysis for carbon, hydrogen and nitrogen was carried out at the University of Queensland by Mr George Blazak or Dr Michael Nefedov.

X-ray crystallography

Crystallographic measurements were carried out using an Oxford Diffraction Gemini Ultra dual source (Mo, $\lambda_{K\alpha}$ = 0.71073 Å and Cu, $\lambda_{K\alpha}$ = 1.5418 Å) CCD diffractometer. Crystal structures were solved by either direct methods (SIR-92) or Patterson's method (SHELX 86) and refined (SHELXL 97) by full matrix least squares methods.[62] These programs were accessed through the WINGX 1.70.01 crystallographic collective package.[63] All non-hydrogen atoms were refined anisotropically unless they were disordered. Hydrogen atoms were fixed geometrically and were not refined. Crystal data are

reported in the ESI.† The X-ray data of the published structures were deposited with the Cambridge Crystallographic Data Centre CCDC 1495702–1495704.

Phosphatase activity measurements

Kinetic measurements of the phosphatase-like activity towards the highly activated substrate bis(2,4-dinitrophenyl) phosphate (BDNPP) were carried out by monitoring the formation of 2,4-dinitrophenol (DNP) at 400 nm. A Varian Cary50 Bio UV/visible spectrophotometer was employed with 10 mm quartz cuvettes and a Peltier temperature controller to maintain a temperature of 298 K. Measurements were taken using a buffer : acetonitrile : DMSO (5 : 4 : 1) solution with a concentration of complex **1** = 0.5 mM and **2** = 0.25 mM. The aqueous buffer consisted of a mixture containing 50 mM MES (2-(*N*-morpholino)ethanesulfonic acid) (pH 5.5–7.0), HEPES (4-(2-hydroxyethyl)-1-piperazineethanesulfonic acid) (pH 6.8–8.2), CHES (2-(*N*-cyclohexylamino)ethane sulfonic acid) (pH 8.6–10.0) and CAPS (*N*-cyclohexyl-3-aminopropanesulfonic acid) (pH 9.7–11.1) at constant ionic strength using 250 mM $LiClO_4$. The pH was adjusted using NaOH to give buffers ranging from pH 6.0 to 11. These were then treated with Chelex for 24 hours and filtered through a 0.45 μm Millex syringe-driven filter. Measurements were carried out as follows: the substrate and the buffer solution were mixed and left for one minute before the addition of the complex. Once the complex was added the reaction was allowed to run for 15 seconds in the measurement chamber for the temperature to stabilize and the reaction to equilibrate. Then the initial rates were determined over a period of three and 10 minutes for complexes **1** and **3**, respectively, by recording the emergence of the 2,4-dinitrophenolate product by its strong absorption at 400 nm (ε = 12 100 M^{-1} cm^{-1});[43] measurements were carried out in triplicate. The pH dependence of the reaction was measured over the range of pH 6.0 to 11. The substrate concentration dependence at optimum pH was also measured and the data were fit to the Michaelis–Menten equation.[64]

Synthesis of the ligands

The ligands HTPDP (HL1) and HTPPNOL (HL2) (Fig. 1) were synthesized as described in the literature.[65,66]

^{1}H NMR (δ/ppm, multiplicity, *J*/Hz): HL1: 8.49–8.45 (4H, m), 7.54 (4H, td, 1.8), 7.37–7.31 (4H, m), 7.12–7.05 (4H, m), 3.98–3.92 (1H, m), 3.81 (8H, s), 2.63 (2H, m), 2.53 (2H, m).^{13}C NMR (δ/ppm): 159.3, 149.0, 136.5, 123.2, 122.1, 67.2, 60.8, 59.1. HL2: 8.52–8.47 (3H, m), 7.66–7.53 (3H, m), 7.35 (1H, d, 7.89), 7.27 (2H, d, 7.89), 7.16–7.08 (3H, m), 4.04–4.00(1H, m), 3.95 (4H, d, 12.06), 3.85 (2H, d, 14.69), 2.83–2.74 (2H, m), 2.71–2.64 (2H, m). ^{13}C NMR (δ/ppm): 159.37, 159.08, 149.07, 148.85, 136.43, 136.42, 123.05, 122.15, 121.99, 121.86, 67.45, 60.42, 59.36, 54.99, 53.15.

CAUTION: some of the compounds prepared below are perchlorate salts of organic–metal complexes and are potentially explosive. Even small amounts of material should be handled with caution.

Synthesis of the complexes

$[Zn(L1)(OAc)](ClO_4)_2$, 1. Zinc(II) perchlorate hexahydrate (2.00 eq., 744.7 mg, 2.00 mmol) was dissolved in MeOH (10 cm^3) and a methanolic solution (10 cm^3) containing HL1 (1.00 eq., 454.6 mg, 1.00 mmol) and sodium acetate (2.00 eq., 164.1 mg, 2.00 mmol) was added. The reaction was stirred under reflux for 30 min. After cooling to room temperature, a white solid was isolated by filtration and washed with diethyl ether. The resulting solid was recrystallized in acetonitrile and colourless crystals (49%, 410.4 mg, 487 μmol) were obtained, which were dried under vacuum. The initial X-ray analysis of a crystal revealed that the cell parameters were identical to those previously reported for the complex.[67] Elemental analysis: Calc. for $C_{29}H_{32}Cl_2N_6O_{11}Zn_2$: C, 41.35; H, 3.83; N, 9.98%. Found: C, 41.86; H, 3.92; N, 9.95%. ^{1}H NMR, (δ/ppm, multiplicity, *J*/Hz): 8.59 (2H, d, 4.8), 8.56 (2H, d, 4.8), 8.17–8.02 (4H, m), 7.70–7.51 (8H, m), 4.35–4.19 (6H, m), 4.02 (2H, d, 17.0), 3.79–3.66 (1H, m), 3.12–3.01 (2H, m), 2.53 (3H, m), 2.04 (2H, t, 11.5). IR: $\bar{\nu}$ = 3630 (w), 3547 (w), 3093 (w), 3039 (w), 2912 (w), 2850 (w), 1609 (m), 1576 (m), 1551 (s), 1486 (m), 1457 (m), 1437 (s), 1424 (s), 1076 (s), 1050 (s), 1027 (s), 767 (s), 621 (s) cm^{-1}.

$[Zn(HL2)](ClO_4)_2$, 2. An ethanolic (15 cm^3) solution containing the ligand HL2 was added to an ethanolic solution (5 cm^3) of $Zn(ClO_4)_2$. The white precipitate which formed was filtered and washed with diethyl ether. Yield: 0.45 g, 0.72 mmol, 72%. The solid was recrystallized in hot MeOH, resulting in crystals suitable for X-ray diffraction. The IR spectra of the crystalline and the amorphous solids were identical. Elemental analysis: Calc. for $C_{21}H_{25}Cl_2N_5O_9Zn$: C, 40.18; H, 4.01; N, 11.16%. Found: C, 40.02; H, 4.08; N, 10.83%. ^{1}H NMR (δ/ppm, multiplicity, *J*/Hz): 8.85 (1H, s), 8.29 (1H, t, 7.1), 8.16–8.08 (4H, m), 7.82–7.78 (2H, m), 7.70 (2H, s), 7.59 (2H, t, 6.4), 5.54–4.96 (2H, m), 4.33–3.58 (6H, m), 3.21–2.74 (3H, m), 3.79–3.66 (1H, m), 3.12–3.01 (2H, m), 2.53 (3H, m), 2.04 (2H, t, 11.5). IR: $\bar{\nu}$ = 3515 (w), 3235 (w), 3077 (w), 2894 (w), 1615 (m), 1577 (w), 1489 (w), 1442 (m), 1071 (s), 1055 (s), 1028 (s), 1010 (s), 768 (s), 758 (s), 619 (s) cm^{-1}.

$[Zn_4(L2)_2(OAc)_3](ClO_4)_3{\cdot}H_2O$, 3. To a methanolic solution (10 cm^3) of $Zn(ClO_4)_2$ (0.830 g, 2.2 mmol,) a MeOH solution (20 cm^3) containing the ligand HL2 (0.390 g, 1,1 mmol) and NaOAc (0.180 g, 2.2 mmol) was added. The mixture was refluxed for 3 h. The reaction was cooled and the solution was allowed to stand in an open beaker for 48 h. The white solid which formed was collected by filtration and washed with diethyl ether. Yield: 0.350 g, 0.24 mmol, 44%. The solid was recrystallized in hot MeOH, resulting in colourless crystals suitable for X-ray diffraction. The IR spectra of the amorphous and the crystalline samples were identical. Elemental analysis: Calc. for $C_{48}H_{59}Cl_3N_{10}O_{21}Zn_4$: C, 38.96; H, 4.02; N, 9.46%. Found: C, 38.79; H, 4.06; N, 9.11%. ^{1}H NMR, (δ/ppm, multiplicity, *J*/Hz): 8.63–8.47 (6H, m), 8.09–7.99 (6H, m), 7.63–7.50 (12H, m), 4.45–3.97 (12H, m), 3.93–3.38 (4H, m), 3.08–2.74 (3H, m), 2.46–2.30 (2H, m), 2.09 (9H, m). IR: $\bar{\nu}$ = 3566 (w), 3324 (w), 3238 (w), 3083 (w), 2937 (w), 2862 (w), 1610 (m), 1577 (m),

1554 (s), 1486 (m), 1437 (s), 1408 (m), 1078 (s), 1054 (s), 1026 (s), 763 (s), 620 (s) cm^{-1}.

Results and discussion

Synthesis and characterization of ligands and complexes

HTPDP (HL1) and HTPPNOL (HL2) (Fig. 1) were synthesized following previously described procedures.[65,66] The NMR spectra of the two ligands (see ESI Fig S1 and S2†) show that the proposed compounds were obtained in high purity. Whilst the aromatic hydrogens of the ligand HL1 exhibited four resonances in the range 7.0–8.5 ppm, in the ligand HL2 these resonances were split into a large number of signals, and the difference was attributed to the lack of symmetry. The same effect could be observed in the ^{13}C spectra. The ligand HL1 exhibited resonances attributed to five aromatic and three aliphatic carbon atoms whilst the spectrum of the ligand HL2 shows resonances attributed to ten aromatic and five aliphatic carbon atoms. Complexes **1** and **3** were prepared by the reaction of $Zn(ClO_4)_2$ in methanol with the appropriate ligand in the presence of sodium acetate; complex **2** was isolated after the reaction of the ligand HL2 and $Zn(ClO_4)_2$ in ethanol.

The nomenclature employed herein follows schemes reported previously for these types of ligands and complexes.[41,65,66,68,69] This approach denotes the number of removable protons upon complexation. Both HTPDP (HL1) and HTPPNOL (HL2) have one potential site for deprotonation; complexation as $L1^-$ and $L2^-$ imply the single deprotonation at the alcohol.

Infrared and NMR spectroscopies

The infrared spectra (see ESI Fig. S3†) of the complexes **1–3** are dominated by the intense perchlorate band (1000–1100 cm^{-1}). The IR spectrum of **2** shows the typical C=N and C=C stretching of the pyridine rings at 1442, 1489, 1577 and 1615 cm^{-1}; **1** and **3** also show similar bands, but they are overlapped by the symmetric and asymmetric stretching of the carboxylate group. For **1** and **3** the υ_{asym} of the COO^- groups are observed at 1551 and 1554 cm^{-1}, respectively. With respect to the υ_{sym}, two intense bands were observed in the range of 1400–1440 cm^{-1} for both complexes (1424 and 1437 cm^{-1} for **1** and 1408 and 1437 cm^{-1} for **3**). Considering any one of these bands, the resulting $\Delta(\upsilon_{asym} - \upsilon_{sym})$ values are in the range observed for bridging carboxylate groups, in agreement with the X-ray molecular structures observed for **1** and **3** (see below). Compound **2** also shows two low intensity broad vibrations at 3235 and 3515 cm^{-1}, which may be attributed to the N–H and O–H stretching; similarly compound **3** displays two bands at 3238 and 3324 cm^{-1} that can be assigned to the N–H vibrations. A secondary amine, as present in complexes **2** and **3**, should show only one N–H vibration. The presence of two such vibrations in **3** may thus indicate the presence of two different N–H groups, a suggestion supported by the X-ray structure.

The complexes were also characterized by ^1H NMR (see ESI Fig. S4†). Compound **1** shows a well resolved spectrum in both aromatic and aliphatic hydrogen regions. Resonances at 2.03 and 3.05 ppm are related to the methylene hydrogen atoms of the 1,3-diaminopropan-2-ol unit. These hydrogen atoms were observed as a multiplet at 2.6 ppm in the free ligand. The methinic hydrogen is observed at 3.72 ppm in the complex and at 3.9 ppm in the free ligand. The methylene protons attached to the pyridine groups are observed at 3.98 to 4.35 ppm as a complex multiplet, while in the free ligand they were observed as a singlet at 3.8 ppm. The resonance at 2.52 ppm, close to the DMSO signal, was attributed to the methyl hydrogen atoms from the acetate group. Interestingly, the hydrogen atoms from the acetate group in the compound $Zn(OAc)_2(H_2O)_2$ are observed at 1.85 ppm (see ESI Fig. S4†). It is known that in this compound the acetate is a bidentate ligand,[70] while in **1** it is a bridging ligand. Therefore, this difference may be ascribed to the different coordination mode of the acetate group in both compounds.

The ^1H NMR spectrum of **2** shows the resolution of the resonances in the aromatic region. However, the aliphatic hydrogen atoms are observed as broad resonances between 2.6 and 5.6 ppm, which indicates a very rigid system. In contrast to the spectrum observed for **1**, no resonance attributed to the acetate moiety was observed. The ^1H NMR spectrum of **3** exhibited lower resolution than the spectra for complexes **1** and **2**. The hydrogen atoms from the acetate groups were observed at 2.09 ppm, different from the chemical shift observed for $Zn(OAc)_2(H_2O)_2$ and complex **1**.

X-ray crystallography

Crystals of all the three complexes synthesized in this work were isolated. An initial X-ray analysis of **1** revealed an unit cell identical to that already reported,[71] in which the ligand HL1 forms a dinuclear zinc complex, as shown in Fig. 1. The molecular structures solved by X-ray diffraction of compounds **2** and **3** are presented in Fig. 2. Structures containing the ligand HL2 have been published previously for iron and copper derivatives. With iron, a tetranuclear complex was obtained,[66] while with copper one dinuclear and two tetranuclear compounds were reported.[72–74]

Although the 1,3-diaminopropan-2-ol unit, present in HL2, usually results in dinuclear complexes, in the presence of one equivalent of the Zn salt, a mononuclear zinc compound was formed (Fig. 2). A similar mononuclear species may be formed when HL2 reacts with copper,[74] but its X-ray molecular structure has not yet been reported. The X-ray structure of **2** reveals the presence of a five-coordinated zinc centre whose coordination environment is composed of the nitrogen donors from the ligand HL2. The zinc centre shows a trigonal-bipyramidal geometry (τ = 0.85)[75] with a plane formed by nitrogen atoms from two pyridine groups and one secondary amine. The bond lengths between these groups and the zinc centre are very similar (2.06 Å). In the axial axis, the zinc is coordinated to a pyridine and a tertiary amine that show longer bond distances (2.128(2) and 2.197(2) Å, respectively) when compared to the

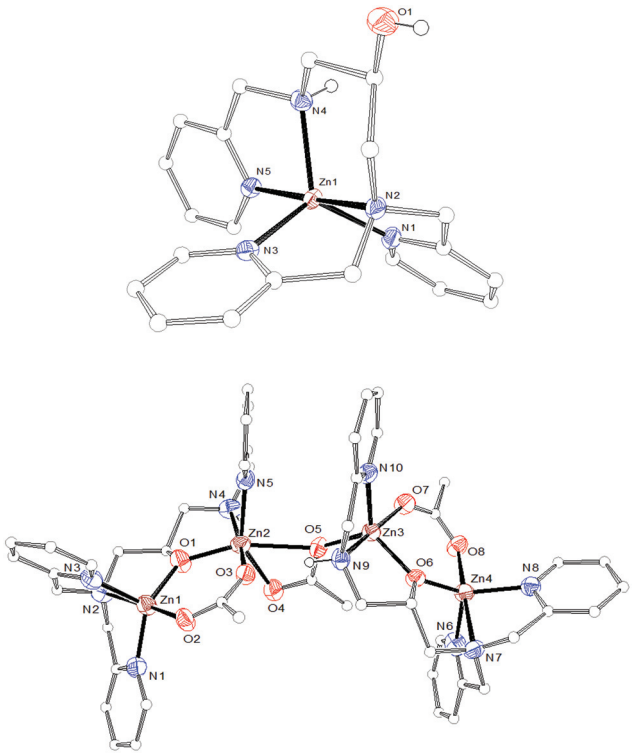

Fig. 2 X-ray molecular structures of complexes **2** (top) and **3** (bottom). Hydrogen atoms and counter ions were omitted for clarity. Main bond lengths for **2** (Å): N(1)–Zn(1) 2.059(2), N(2)–Zn(1) 2.197(2), N(3)–Zn(1) 2.063(2). Main bond lengths for **3** (Å): N(1)–Zn(1) 2.059(6), N(2)–Zn(1) 2.227(5), N(3)–Zn(1) 2.057(6), N(6)–Zn(4) 2.042(6), N(7)–Zn(4) 2.256(6), N(8)–Zn(4) 2.061(5), Zn(1)–Zn(2) 3.465(5), Zn(3)–Zn(4) 3.484(5), Zn(2)–Zn(3) 4.106(5). Main bond angles for **2** (°): N(1)–Zn(1)–N(3) 123.09(10), N(1)–Zn(1)–N(2) 79.74(9), N(3)–Zn(1)–N(2) 79.75(9). Main bond angles for **3** (°): N(1)–Zn(1)–N(3) 113.7(2), N(1)–Zn(1)–N(2) 78.9(2), N(3)–Zn(1)–N(2) 79.7(2), N(6)–Zn(4)–N(8) 110.3(2), N(6)–Zn(4)–N(7) 79.1(3), N(8)–Zn(4)–N(7) 78.1(2).

bonds present in the plane. The alcohol group is not interacting with the zinc centre. The structure shows three five-membered chelate rings, whose ligand–metal–ligand angles are close to 80 degrees, and one six-membered ring, with a corresponding angle of 95.9°.

While the reaction of the zinc salt with the hepta-dentate ligand HL1 in a stoichiometry of 2 : 1 results in the formation of the dinuclear complex **1**, the X-ray analysis of the crystal obtained for the same reaction conditions, but in the presence of HL2, revealed a tetranuclear species (Fig. 2) composed of two dinuclear units (A and B) of the composition $Zn_2L(OAc)$; their inter-dimer Zn–Zn interaction is promoted by an acetate bridge that acts as a monodentate ligand to one of the Zn(II) ions but binds in a bidentate manner to the other (coordination mode μ_2:η^2–η^1), while within one unit the two metals are bridged by an alkoxide and an acetate group. The metal ions in the Zn1 and Zn4 positions have the same geometry (trigonal-bipyramidal, τ = 0.8 and 0.9, respectively)[75] and coordination environment (N_3O_2). The Zn3 site also has a trigonal-bipyramidal geometry, but with an N_2O_3 coordination environment. Due to the asymmetric coordination of the inter-dimer acetate bridge the Zn2 site has an N_2O_4 coordination environment.

Kinetic studies

Phosphatase-like activities of **1** and **3** were measured using the activated substrate BDNPP, and the dependence of the catalytic rate on pH was determined in the pH range 6 to 11 (Fig. 3); **2** was not active under the conditions employed. Relevant parameters are summarized in Table 1. Previous studies[42,49,50,52,54,57,76] support the underlying assumption made here that the bridging acetates dissociate in an aqueous environment, and this dissociation provides the binding sites for the substrate and water molecules from the solvent. Compound **3** is very soluble in acetonitrile, in a 1 : 1 mixture with aqueous buffer a cloudy precipitate appeared. This problem was overcome when the complex was dissolved in DMSO instead. However, to avoid precipitation the sequence of addition of the components differs from the usual approach, where the substrate is added to the solution (buffer : acetonitrile) that contains the complex.[39,41,42,53] Here, a DMSO solution of the complexes (0.1 cm^3) was added to the buffered solution containing the substrate (0.5 cm^3 buffer, 0.4 cm^3 of acetonitrile). Consequently, the kinetic experiments were performed in a 5 : 4 : 1 buffer : acetonitrile : DMSO mixture. For **1**, the data were collected during the first 180 s where a linear increase in the absorption was observed. Complex **3**, however, displayed distinctly different behaviour (Fig. 4). After an initial burst phase lasting ~60 s the reaction rate gradually leveled off, reaching a steady-state after ~120 s. Such a behaviour has been observed, amongst others, for the peptidase chymotrypsin,[77] it is reminiscent of the effect of slow binding inhibitors such as fluoride to PAPs[78] and may be associated with a structural rearrangement induced by the initial interaction between BDNPP and the catalyst. Therefore, the kinetic data for **3** were obtained after 120 s.

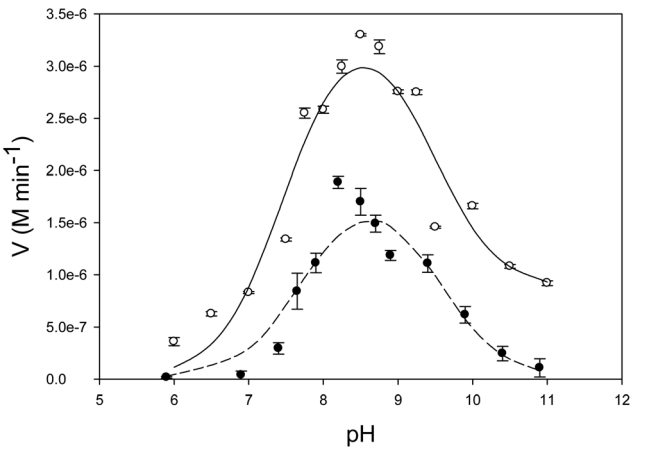

Fig. 3 Dependence of phosphatase activity on the pH for **1** (○) and **3** (●). [BDNPP] = 4.2 mM, [**1**] = 0.5 mM, [**2**] = 0.25 mM. Buffer : acetonitrile : DMSO (5 : 4 : 1) with 50 mM MES, HEPES, CHES and CAPS, and 250 mM $LiClO_4$, at 25 °C.

Table 1 Kinetic data and pK_a values for **1** and **3**

Compound	pK_{a1}	pK_{a2}	V_{max} (M min^{-1})	K_m (mM)	k_{cat} (min^{-1})	k_{cat}/K_m (M^{-1} min^{-1})
1	7.47	9.46	$1.57 \pm 0.08 \times 10^{-5}$	8.2 ± 0.4	31.4×10^{-3}	3.8
3	7.72	9.54	$3.86 \pm 0.6 \times 10^{-6}$	4.4 ± 1	7.7×10^{-3}	1.8

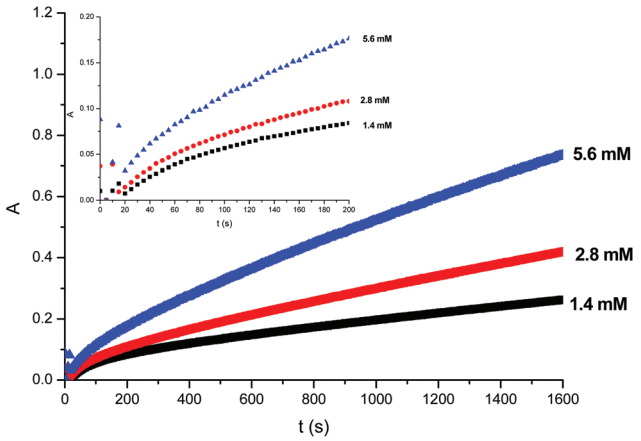

Fig. 4 Plot of absorption *vs.* time in the reaction of BDNPP with **3** followed at 400 nm. Substrate concentrations are indicated on the right, [**3**] = 0.25 mM. Buffer : acetonitrile : DMSO (5 : 4 : 1) with 50 mM MES, HEPES, CHES and CAPS, and 250 mM $LiClO_4$, at 25 °C and pH 8.5. The inset shows the first 200 s of the reaction progress curve.

The pH rate profiles for the two complexes **1** and **3** were different. While a bell-shaped behaviour is observed for both with a pH optimum at ~pH 8.5, for **1** the rate appeared to approach a limiting rate above pH 11, while **3** is inactive at high pH. For **1**, the data were fitted to eqn (1),[64,79]

$$v_0 = \frac{v_{max}\left(1 + \frac{\kappa K_{a2}}{[H^+]}\right)}{\left(1 + \frac{[H^+]}{K_{a1}} + \frac{K_{a2}}{[H^+]}\right)} \quad (1)$$

resulting in pK_{a1} = 7.47 and pK_{a2} = 9.46, with κ = 0.2446 being the ratio of the limiting rate at high pH and the rate at optimum pH. The data for **3** were fitted to eqn (2) (where κ = 0),[64,79]

$$v_0 = \frac{v_{max}}{\left(1 + \frac{[H^+]}{K_{a1}}\right) + \frac{K_{a2}}{[H^+]}} \quad (2)$$

with pK_{a1} = 7.72 and pK_{a2} = 9.54. In both complexes the two pK_as are likely to be associated with Zn(II)-bound water molecules. A plausible interpretation associates pK_{a1} with the nucleophilic hydroxide that initiates hydrolysis, while pK_{a2} may be ascribed to a water molecule that obstructs substrate coordination due to slow ligand exchange (in its deprotonated form). The relative acidic value of pK_{a1}, together with its significant difference from pK_{a2} (~2 pH units) suggests that its associated residue may be a metal ion-bridging water, while the residue ascribed to pK_{a2} may be a terminally coordinated water. The effect of the substrate concentration on the catalytic rate of the two complexes was evaluated at optimum pH (*i.e.* pH 8.5; Fig. 3). Both data sets display saturation behaviour and were thus fitted to the Michaelis–Menten equation (Fig. 5 and Table 1). While complex **1** is approximately four-fold more reactive than complex **3**, its affinity (estimated by the K_m value) for the substrate is reduced. Consequently, **1** is approximately twice as efficient a catalyst as **3** (as judged by the k_{cat}/K_m ratio).

The main difference in the catalytic behaviour of the two complexes appears to be the number of possible active species; while for **1** both the singly- and doubly-deprotonated species display catalytic activity (with the former approximately four-fold faster), for **3** only the singly-deprotonated species is active. Behaviour similar to that of **1** was observed previously.[41,79–81] In contrast, we are not aware of other di-zinc(II) complexes that display an initial kinetic burst as observed for **3** (Fig. 4). Since the initial rate (estimated from the tangent at t = 0 in Fig. 4) during the burst phase approximates the steady-state rate recorded for **1** under similar experimental conditions, it is possible that a dinuclear "half" of **3** (*i.e.* $[Zn_2(L2)(H_2O)_n]^{3+}$) may be present as the active species; gradual formation of the tetrameric complex leads to the observed change in the catalytic rate. Alternatively, the complex may adopt two distinct conformations, one that is more accessible to the substrate and hence promotes a more rapid turnover, and one that is more secluded. While the kinetic data do not allow

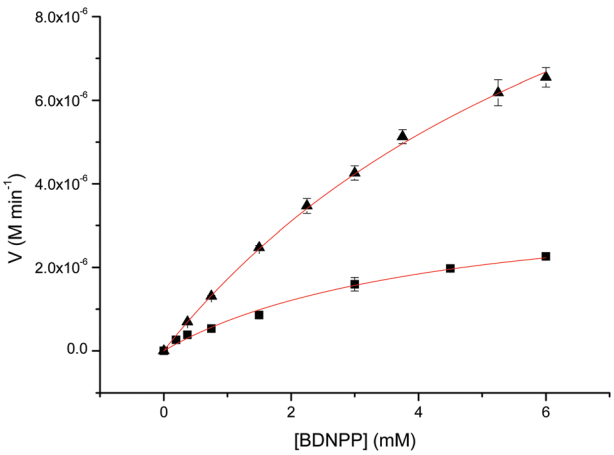

Fig. 5 Substrate dependence measured at pH 8.5 for 0.5 mM **1** (▲) and 0.25 mM **3** (■), buffer : acetonitrile : DMSO (5 : 4 : 1) with 50 mM MES, HEPES, CHES and CAPS, and 250 mM $LiClO_4$, at 25 °C.

a distinction between these two possibilities, crystallographic information discussed below favors the latter mechanism.

^{31}P NMR studies

In order to probe the details of the catalytic reactions promoted by **1** and **3** further ^{31}P NMR was employed. Initially, the interactions between **1** and several phosphate species (*i.e.* PO_4^{3-}, 4NPP, B4NPP) were monitored under conditions similar to those used in the kinetic assays (in a buffer : CD_3CN : DMSO-d_6 (5 : 4 : 1) mixture at pH 8.5, but with a complex : reactant ratio of 1 : 1). Under these conditions the phosphate ion PO_4^{3-} displays a resonance at ~2.7 ppm (Fig. 6(a)). When complex **1** is added this signal almost disappears but new resonances at 3.50, 3.57, 11.30 and 11.35 ppm emerge (Fig. 6(b)). The resonances around 11.3 ppm account for ~75% of the phosphate species in solution, whilst the resonances around 3.5 ppm represent ~20% of the phosphate content. The observation of these new resonances after addition of **1** supports the coordination of phosphate to the metal ions of the complex. The more moderately perturbed resonances around 3.5 ppm are, tentatively,

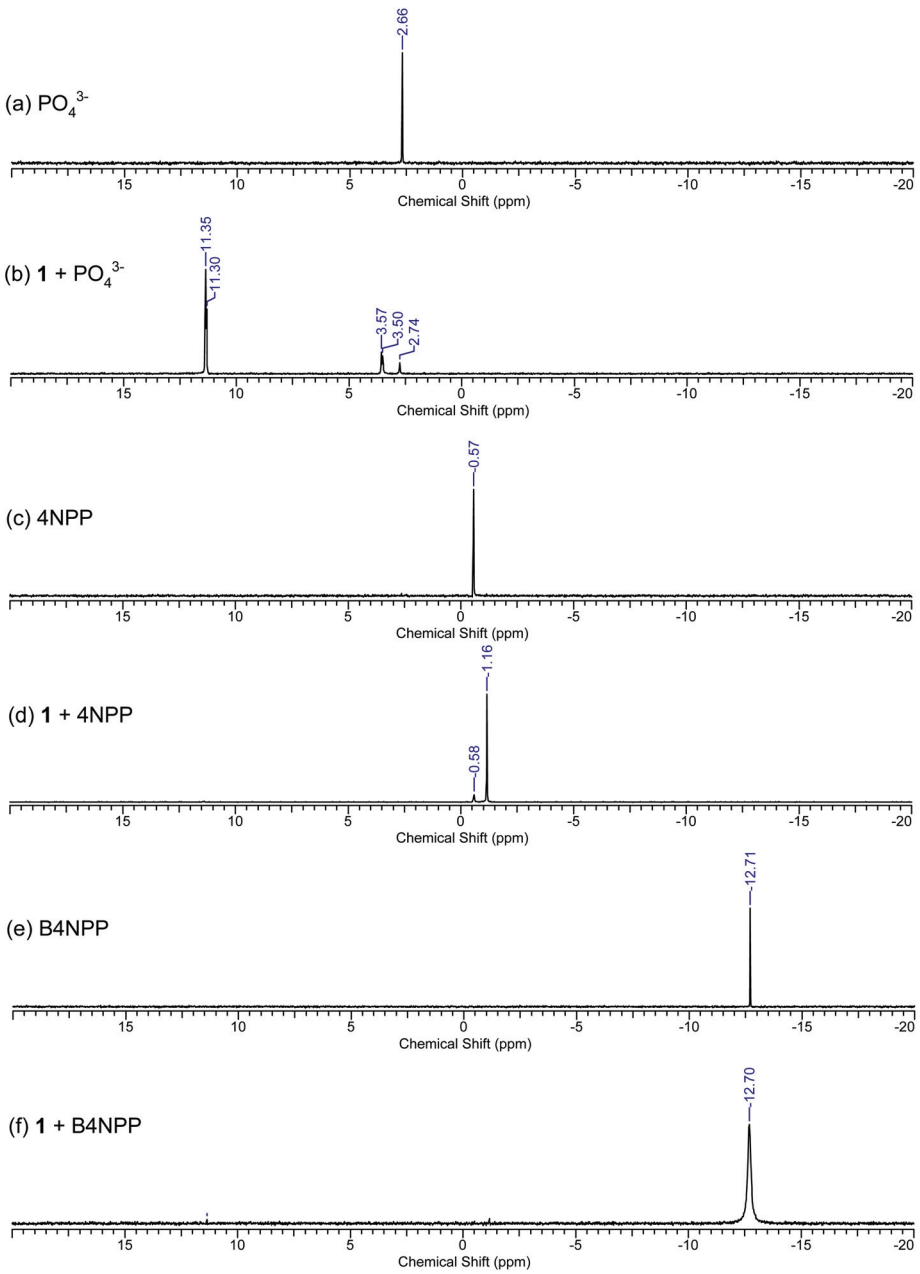

Fig. 6 ^{31}P NMR spectra of phosphate (PO_4^{3-}), 4-nitrophenylphosphate (4NPP) and bis(4-nitrophenyl)phosphate (B4NPP) in the absence and in the presence of complex **1** at a stoichiometry 1 : 1, at pH 8.5, in CD_3CN : buffer : DMSO-d_6 (4 : 5 : 1), after 24 h.

assigned to the coordination of the phosphate ion as a monodentate ligand to either of the Zn(II); in contrast, the more significantly perturbed resonances around 11.3 ppm are attributed to the coordination of the phosphate ion as a bidentate, metal ion-bridging ligand. In the case of the monoester 4NPP alone a resonance at −0.57 ppm is observed, which practically disappears after the addition of the complex (Fig. 6(c) and (d)). However, a new signal that represents 86% of the phosphorus species is observed at −1.16 ppm. It was previously reported that 4NPP has a resonance at −5.05 ppm in CD_3CN that undergoes a downfield shift to 0.62 ppm after coordination as a bridging group (μ_2:η^1–η^1).[47] Thus, the considerably smaller shift observed here (from −0.57 to −1.16) may suggest a monodentate coordination mode for this ligand. Lastly, in the case of the diester B4NPP the resonance of the phosphorus nucleus in solution is observed at −12.7 ppm (Fig. 6(e)) and does not change in the presence of complex **1** (Fig. 6(f)), suggesting that this reactant does not interact with the zinc ions. This interpretation is in agreement with the observed lack of activity of both **1** and **3** towards B4NPP.

In contrast to B4NPP, 2,4-BDNPP does not only bind to the metal centre of both complexes, but it is also hydrolyzed. Fig. 7 shows the time-dependent ^{31}P NMR spectra of the reactions between complexes **1** and **3** with 2,4-BDNPP (recorded under stoichiometric conditions). For both complexes the initial spectra are dominated by the resonance attributed to unbound 2,4-BDNPP at −14.10 ppm. After 24 h, a new intense signal (52%) around −0.1 ppm is observed for the reaction containing complex **1**. From a comparison with the data presented above (Fig. 6) and also with the data described in the literature,[47] this resonance is attributed to the monoester 2,4-DNPP. In addition, a resonance at 11.9 ppm is also emerging after 24 h. This signal is close to those observed when complex **1** is incubated with the phosphate anion alone (Fig. 6(b)), indicating that **1** is capable of hydrolyzing both the ester bonds of 2,4-BDNPP. Based on the estimated rates of DNPP and phosphate formation (from an analysis of the peak areas of relevant resonances shown in Fig. 7) the hydrolysis of the two ester bonds is likely to occur in a processive manner as observed for PAPs (DNPP is less activated than BDNPP and thus a very poor substrate, preventing accurate kinetic measurements under the same experimental conditions).[82,83] DNPP formation is most rapid in the first 24 hours of the reaction (its contribution to the NMR resonances increases from 0 to 52.5%) before slowing down significantly (with increases of 6.5% and 6% over the following 24 and 72 hours, respectively). In contrast, the rate of phosphate formation remains virtually constant over the entire 120 hours, increasing in species contribution by approximately 2% per day.

For the reaction with complex **3** a feature around −0.5 ppm emerges; after 24 hours of incubation this feature accounts for

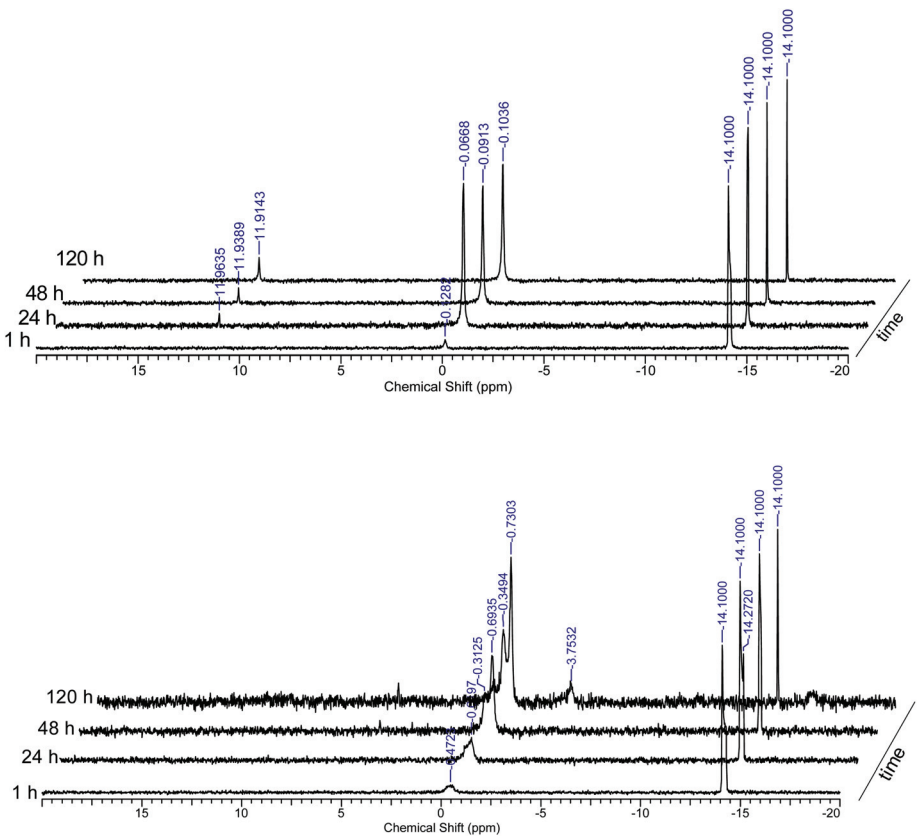

Fig. 7 ^{31}P NMR spectra at different times of the reactions between complexes **1** (top) and **3** (bottom) with 2,4-BDNPP.

30% of phosphorus in the sample. This resonance is also likely to be associated with the coordinated monoester 2,4-DNPP. As more of this product is accumulated the spectral feature is clearly resolved into two distinct bands at ~−0.3 and ~−0.7 ppm (Fig. 7). A similar splitting of resonances has been previously observed in phosphate-containing complexes and may be due to the presence of different conformers;[47] phosphorus resonances are influenced by O–P–O angles and the torsional angles R–O–P–O(R).[84] An additional broad resonance appears at −3.75 ppm after several days. While the origin of this resonance is currently obscure it is important to point out that no resonances are observed that may be assigned to the presence of phosphate (as observed for the reaction with **1**). Hence, in contrast to **1** complex **3** does not appear to be able to hydrolyze monoester substrates.

X-ray structural characterization of the product of the reaction between 3 and BDNPP

While monitoring the catalytic reaction between **3** and BDNPP we observed the formation of crystals. Using X-ray diffraction it could be shown that a tetranuclear species, $[Zn_4(L2)_2(DNPP)_2](ClO_4)_2$, **4**, is formed. Its molecular structure is shown in Fig. 8 and relevant crystallographic parameters, bond lengths and angles are summarised in Tables S1–S3 (ESI†). The complex consists of two Zn_2L2 subunits, connected *via* two DNPP molecules. DNPP, as mentioned above, is the product of the hydrolysis of BDNPP. The four zinc(II) ions display distorted trigonal-bipyramidal geometry, with two metal ions possessing a N_3O_2 donor set and the remaining two a N_2O_3 environment. The tetranuclear species has a centre of inversion. While Zn(1) is coordinated by only one oxygen atom from the phosphate moiety, Zn(2) is coordinated by two oxygen atoms located on two different phosphate groups. Furthermore, while **3** has an open structure, complex **4** adopts a more closed configuration, resembling a parallelogram with Zn···Zn distances of 3.612 Å (intradimer) and 5.671 Å (interdimer) (see also Fig. 1). The intradimer Zn1···Zn2 distance is longer in **4** than in **3** (3.612 *vs.* 3.466 and 3.448 Å), which may be due to different bridging groups in the two complexes (phosphate *vs.* carboxylate). This elongated metal–metal distance also results in a more opened alkoxide bridge in **4** in comparison with **3**. In the latter, the Zn–OR–Zn angles are 125.88° and 126.10°, while an angle of 130.87° is observed for **4**. The same effect is observed when complex **1** reacts with PNPP, resulting in the compound $[Zn_2(L1)(PNPP)]^+$; the relevant angle increases from 123° to 129.8°.[67]

The crystal structure of **4** illustrates that two phosphate monoesters are tightly coordinated to the zinc centres with an unusual coordination mode, μ–η^1:η^1:η^1, in which the three oxygen atoms of DNPP interact with three distinct metal ions. To our knowledge the only other known example of a phosphate complex whereby three oxygen atoms of the ligand bind to three different metal ions is the compound $[Zn_3(CF_3SO_3)_3(\mu_3\text{-}HPO_4)L](CF_3SO_3)$.[85] This tight coordination of DNPP may account for the lack of phosphate formation by **3** (Fig. 7).

No crystals from the reaction between **1** and BDNPP were obtained, possibly due to the fact that **1** also hydrolyses DNPP (Fig. 7). However, the crystal structure of the complex between **1** and the monoester 4NPP was previously reported.[67] A dinuclear species was formed, in which the phosphate moiety of PNPP replaced the bridging acetate.

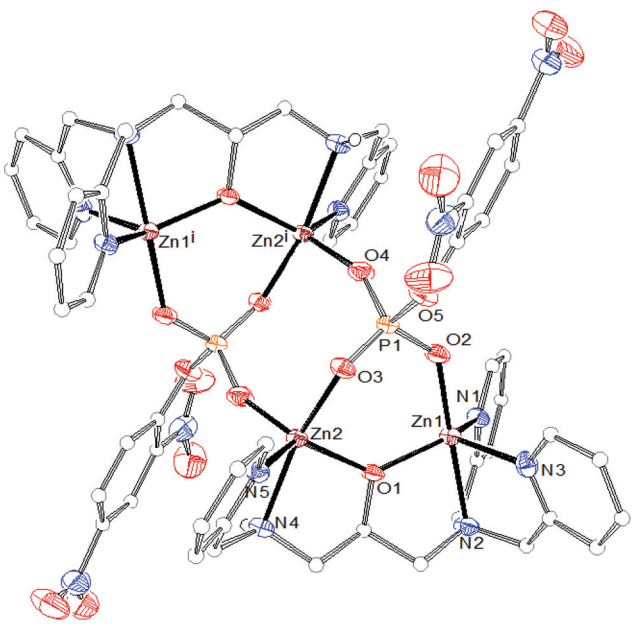

Fig. 8 X-ray molecular structure of complex **4**. Hydrogen atoms and counter ions were omitted for clarity. Main bond lengths for **4** (Å): N(1)–Zn(1) 2.068(3), N(2)–Zn(1) 2.250(3), N(3)–Zn(1) 2.088(4), Zn(1)–Zn(2) 3.612(3), Zn(1)–Zn(2)^i 5.670(3), Zn(1)–Zn(1)^i 8.170(3), Zn(2)–Zn(2)^i 4.863(3). Main bond angles for **4** (°): N(1)–Zn(1)–N(3) 107.97(13), N(1)–Zn(1)–N(2) 77.96(13); N(3)–Zn(1)–N(2) 78.74(14).

Conclusions

In this study we compared the ligands HL1 (hepta-dentate) and HL2 (hexa-dentate) with respect to their coordination behaviour with zinc(II). While a dinuclear zinc compound was formed with the former (complex **1**), the latter resulted in either a mononuclear (complex **2**) or tetranuclear (complex **3**) species, depending on the amount of metal ions added. Compound **2** is catalytically inactive, possibly because it does not provide an adequate binding site for the substrate. Compound **1** displays the highest steady-state rate (Table 1), but in the initial burst phase **3** has a rate similar to that of **1** (Fig. 4). Based on the comparison of the crystal structures of free **3** and product-bound **3** (Fig. 1, 2 and 8) it is likely that the initial substrate (*i.e.* BDNPP) binding triggers a structural change in **3** from a more substrate-accessible to a rather secluded conformation. This interpretation implies that **3** mimics not only the catalytic activity of metallohydrolases such as PAPs, but also some of the conformational flexibility inherent to enzyme-catalysed reactions. With respect to the catalytic mechanism compounds **1** and **3** are similar, display-

ing the maximum activity at ~pH 8.5. A nucleophile with a pK_a of ~7.5 (Table 1) is identified as the species initiating hydrolysis. A doubly-Lewis activated water molecule bridging two zinc ions would be a plausible candidate for such a nucleophilic species, an assignment that is in agreement with numerous studies on metallohydrolase enzymes.[1,2] A second catalytically-relevant pK_a (~9.5; Table 1) is observed for both active compounds. A water molecule coordinated to only one Zn(II) would be anticipated to possess an acid dissociation constant of this magnitude, as observed in a multitude of related metallosystems.[16,26,28,29,52,86–90] Interestingly, while the deprotonation of this water ligand abolishes the catalytic activity of **3**, compound **1** maintains residual activity at high pH (Fig. 3). This may suggest that in **1** the substrate can bind in two alternative modes to the metal centre, bridging and terminally coordinated, while in **3** only the bridging mode is observed. This difference may also account for the observation that the former promotes the cleavage of both the ester bonds in BDNPP whereas the latter only hydrolyses one, as observed in the ^{31}P NMR data (Fig. 7). It is interesting to note that PAP also has the ability to cleave both the ester bonds in diester substrates in a processive manner.[82]

In summary, the comparative study of two ligand systems demonstrated that both may reconstitute features characteristic of metallohydrolases such as PAPs. Both are catalytically active towards the diester substrate BDNPP, and while **1** mimics the processive hydrolysis of both ester bonds, **3** may demonstrate structural flexibility as observed in its burst kinetics. The next challenge towards building more efficient biomimetics will be combining these features into one system. Efforts towards this goal are currently in progress.

Acknowledgements

The authors acknowledge the financial support received from Brazilian funding agencies CNPq (406749/2013-2) and CAPES (99999.006336/2014-00), as well as a grant from the Australian Research Council (DP150104358). GS also acknowledges the Australian Research Council for the award of a Future Fellowship (FT120100694). The authors also acknowledge the assistance of Prof. Paul V. Bernhardt in collecting the X-ray diffraction data.

References

1 N. Mitić, S. J. Smith, A. Neves, L. W. Guddat, L. R. Gahan and G. Schenk, *Chem. Rev.*, 2006, **106**, 3338–3363.
2 G. Schenk, N. Mitic, L. R. Gahan, D. L. Ollis, R. P. McGeary and L. W. Guddat, *Acc. Chem. Res.*, 2012, **45**, 1593–1603.
3 M. W. Crowder, J. Spencer and A. J. Vila, *Acc. Chem. Res.*, 2006, **39**, 721–728.
4 G. Schenk, I. Mateen, T.-K. Ng, M. M. Pedroso, N. Mitic, M. Jafelicci, R. F. C. Marques, L. R. Gahan and D. L. Ollis, *Coord. Chem. Rev.*, 2016, **317**, 122–131.
5 N. Mitić, M. Miraula, C. Selleck, K. S. Hadler, M. M. Pedroso, E. Uribe and G. Schenk, *Adv. Protein Chem. Struct. Biol.*, 2014, **97**, 49–81.
6 D. M. F. van Aalten, C. R. Chong and L. Joshua-Tor, *Biochemistry*, 2000, **39**, 10082–10089.
7 D. W. Christianson and W. N. Lipscomb, *Acc. Chem. Res.*, 1989, **22**, 62–69.
8 M. A. Holmes and B. W. Matthews, *J. Mol. Biol.*, 1982, **160**, 623–639.
9 O. A. Adekoya and I. Sylte, *Chem. Biol. Drug Des.*, 2009, **73**, 7–16.
10 B. W. Matthews, *Acc. Chem. Res.*, 1988, **21**, 333–340.
11 J. E. Coleman, *Curr. Opin. Chem. Biol.*, 1998, **2**, 222–234.
12 B. Krajewska, *J. Mol. Catal. B: Enzym.*, 2009, **59**, 9–21.
13 E. Jabri, M. B. Carr, R. P. Hausinger and P. A. Karplus, *Science*, 1995, **268**, 998–1004.
14 G. C. Dismukes, *Chem. Rev.*, 1996, **96**, 2909–2926.
15 G. Schenk, N. Mitic, G. R. Hanson and P. Comba, *Coord. Chem. Rev.*, 2013, **257**, 473–482.
16 N. Mitic, K. S. Hadler, L. R. Gahan, A. C. Hengge and G. Schenk, *J. Am. Chem. Soc.*, 2010, **132**, 7049–7054.
17 P. V. Bernhardt, G. Schenk and G. J. Wilson, *Biochemistry*, 2004, **43**, 10387–10392.
18 J. L. Millan, *Purinergic Signalling*, 2006, **2**, 335–341.
19 W. Yang, *Q. Rev. Biophys.*, 2011, **44**, 1–93.
20 Y. Gao, Y. B. Truong, P. Cacioli, P. Butler and I. L. Kyratzis, *Enzyme Microb. Technol.*, 2014, **54**, 38–44.
21 F. Ely, K. S. Hadler, N. Mitić, L. R. Gahan, D. L. Ollis, J. A. Larrabee and G. Schenk, *J. Biol. Inorg. Chem.*, 2011, **16**, 777–787.
22 R. Arai, K. Ito, T. Ohnishi, H. Ohba, R. Akasaka, Y. Bessho, K. Hanawa-Suetsugu, T. Yoshikawa, M. Shirouzu and S. Yokoyama, *Proteins: Struct., Funct., Bioinf.*, 2007, **67**, 732–742.
23 L. J. Daumann, J. A. Larrabee, D. Ollis, G. Schenk and L. R. Gahan, *J. Inorg. Biochem.*, 2014, **131**, 1–7.
24 J. Weston, *Chem. Rev.*, 2005, **105**, 2151–2174.
25 A. N. Bigley and F. M. Raushel, *Biochim. Biophys. Acta*, 2013, **1834**, 443–453.
26 K. S. Hadler, N. Mitic, F. Ely, G. R. Hanson, L. R. Gahan, J. A. Larrabee, D. L. Ollis and G. Schenk, *J. Am. Chem. Soc.*, 2009, **131**, 11900–11908.
27 E. Ghanem and F. M. Raushel, *Toxicol. Appl. Pharmacol.*, 2005, **207**, S459–S470.
28 G. Schenk, R. A. Peralta, S. C. Batista, A. J. Bortoluzzi, B. Szpoganicz, A. K. Dick, P. Herrald, G. R. Hanson, R. K. Szilagyi, M. J. Riley, L. R. Gahan and A. Neves, *J. Biol. Inorg. Chem.*, 2008, **13**, 139–155.
29 S. J. Smith, R. A. Peralta, R. Jovito, A. Horn, A. J. Bortoluzzi, C. J. Noble, G. R. Hanson, R. Stranger, V. Jayaratne, G. Cavigliasso, L. R. Gahan, G. Schenk, O. R. Nascimento, A. Cavalett, T. Bortolotto, G. Razzera, H. Terenzi, A. Neves and M. J. Riley, *Inorg. Chem.*, 2012, **51**, 2065–2078.
30 A. Horn Jr., C. Fernandes, G. L. Parrilha, M. M. Kanashiro, F. V. Borges, E. J. T. de Melo, G. Schenk, H. Terenzi and C. T. Pich, *J. Inorg. Biochem.*, 2013, **128**, 38–47.

31 A. Horn, I. Vencato, A. J. Bortoluzzi, R. Horner, R. A. N. Silva, B. Spoganicz, V. Drago, H. Terenzi, M. C. B. de Oliveira, R. Werner, W. Haase and A. Neves, *Inorg. Chim. Acta*, 2005, **358**, 339–351.
32 B. de Souza, R. Heying, A. J. Bortoluzzi, J. B. Domingos and A. Neves, *J. Mol. Catal. A: Chem.*, 2015, **397**, 76–84.
33 L. Zhang, B. Li, X. Meng, L. Huang and D. Wang, *Environ. Sci. Pollut. Res.*, 2015, **22**, 15104–15112.
34 E. Ghanem, Y. Li, C. Xu and F. M. Raushel, *Biochemistry*, 2007, **46**, 9032–9040.
35 C. Piovezan, R. Jovito, A. J. Bortoluzzi, H. Terenzi, F. L. Fischer, P. C. Severino, C. T. Pich, G. G. Azzolini, R. A. Peralta, L. M. Rossi and A. Neves, *Inorg. Chem.*, 2010, **49**, 2580–2582.
36 B. de Souza, G. L. Kreft, T. Bortolotto, H. Terenzi, A. J. Bortoluzzi, E. E. Castellano, R. A. Peralta, J. B. Domingos and A. Neves, *Inorg. Chem.*, 2013, **52**, 3594–3596.
37 A. Neves, M. A. de Brito, I. Vencato, V. Drago, K. Griesar, W. Haase and Y. P. Mascarenhas, *Inorg. Chim. Acta*, 1993, **214**, 5–8.
38 A. Neves, M. A. deBrito, I. Vencato, V. Drago, K. Griesar and W. Haase, *Inorg. Chem.*, 1996, **35**, 2360–2368.
39 L. R. Gahan, S. J. Smith, A. Neves and G. Schenk, *Eur. J. Inorg. Chem.*, 2009, **19**, 2745–2758.
40 A. Neves, M. A. de Brito, V. Drago, K. Griesar and W. Haase, *Inorg. Chim. Acta*, 1995, **237**, 131–135.
41 L. J. Daumann, L. Marty, G. Schenk and L. R. Gahan, *Dalton Trans.*, 2013, **42**, 9574–9584.
42 A. E. Roberts, G. Schenk and L. R. Gahan, *Eur. J. Inorg. Chem.*, 2015, **2015**, 3076–3086.
43 R. A. Peralta, A. J. Bortoluzzi, B. de Souza, R. Jovito, F. R. Xavier, R. A. Couto, A. Casellato, F. Nome, A. Dick, L. R. Gahan, G. Schenk, G. R. Hanson, F. C. de Paula, E. C. Pereira-Maia, P. M. S. de, P. C. Severino, C. Pich, T. Bortolotto, H. Terenzi, E. E. Castellano, A. Neves and M. J. Riley, *Inorg. Chem.*, 2010, **49**, 11421–11438.
44 P. V. Bernhardt, S. Bosch, P. Comba, L. R. Gahan, G. R. Hanson, V. Mereacre, C. J. Noble, A. K. Powell, G. Schenk and H. Wadepohl, *Inorg. Chem.*, 2015, **54**, 7249–7263.
45 M. Ghiladi, C. J. McKenzie, A. Meier, A. K. Powell, J. Ulstrup and S. Wocadlo, *J. Chem. Soc., Dalton Trans.*, 1997, 4011–4018.
46 S. Bosch, P. Comba, L. R. Gahan and G. Schenk, *J. Inorg. Biochem.*, 2016, **162**, 343–355.
47 S. Bosch, P. Comba, L. R. Gahan and G. Schenk, *Inorg. Chem.*, 2014, **53**, 9036–9051.
48 P. Comba, L. R. Gahan, G. R. Hanson, V. Mereacre, C. J. Noble, A. K. Powell, I. Prisecaru, G. Schenk and M. Zajaczkowski-Fischer, *Chem. – Eur. J.*, 2012, **18**, 1700–1710.
49 F. R. Xavier, A. J. Bortoluzzi and A. Neves, *Chem. Biodiversity*, 2012, **9**, 1794–1805.
50 F. R. Xavier, R. A. Peralta, A. J. Bortoluzzi, V. Drago, E. E. Castellano, W. Haase, Z. Tomkowicz and A. Neves, *J. Inorg. Biochem.*, 2011, **105**, 1740–1752.
51 P. Karsten, A. Neves, A. J. Bortoluzzi, M. Lanznaster and V. Drago, *Inorg. Chem.*, 2002, **41**, 4624–4626.
52 F. R. Xavier, A. Neves, A. Casellato, R. A. Peralta, A. J. Bortoluzzi, B. Szpoganicz, P. C. Severino, H. Terenzi, Z. Tomkowicz, S. Ostrovsky, W. Haase, A. Ozarowski, J. Krzystek, J. Telser, G. Schenk and L. R. Gahan, *Inorg. Chem.*, 2009, **48**, 7905–7921.
53 L. J. Daumann, *Spectroscopic and Mechanistic Studies of Dinuclear Metallohydrolases and their Biomimetic Complexes*, Springer International Publishing, Switzerland, 2014.
54 B. Das, H. Daver, A. Singh, R. Singh, M. Haukka, S. Demeshko, F. Meyer, G. Lisensky, M. Jarenmark, F. Himo and E. Nordlander, *Eur. J. Inorg. Chem.*, 2014, **2014**, 2204–2212.
55 M. Lanznaster, A. Neves, A. J. Bortoluzzi, B. Szpoganicz and E. Schwingel, *Inorg. Chem.*, 2002, **41**, 5641–5643.
56 S. J. Smith, M. J. Riley, C. J. Noble, G. R. Hanson, R. Stranger, V. Jayaratne, G. Cavigliasso, G. Schenk and L. R. Gahan, *Inorg. Chem.*, 2009, **48**, 10036–10048.
57 S. Drueke, K. Wieghardt, B. Nuber, J. Weiss, H. P. Fleischhauer, S. Gehring and W. Haase, *J. Am. Chem. Soc.*, 1989, **111**, 8622–8631.
58 R. Than, A. A. Feldmann and B. Krebs, *Coord. Chem. Rev.*, 1999, **182**, 211–241.
59 A. Neves, S. M. D. Erthal, V. Drago, K. Griesar and W. Haase, *Inorg. Chim. Acta*, 1992, **197**, 121–124.
60 A. Neves, L. M. Rossi, A. Horn Jr., I. Vencato, A. J. Bortoluzzi, C. Zucco and A. S. Mangrich, *Inorg. Chem. Commun.*, 1999, **2**, 334–337.
61 L. M. Rossi, A. Neves, A. J. Bortoluzzi, R. Horner, B. Szpoganicz, H. Terenzi, A. S. Mangrich, E. Pereira-Maia, E. E. Castellano and W. Haase, *Inorg. Chim. Acta*, 2005, **358**, 1807–1822.
62 G. M. Sheldrick, *SHELXL97: Program for the refinement of crystal structures*, University of Gottingen, Germany, 1997.
63 L. J. Farrugia, *J. Appl. Crystallogr.*, 1999, **32**, 837–838.
64 I. H. Segel, *Enzyme kinetics: behavior and analysis of rapid equilibrium and steady state enzyme systems*, Wiley-Interscience, New York, 1975.
65 M. Sato, Y. Mori and T. Iida, *Synthesis*, 1992, 539–540.
66 C. Fernandes, A. Neves, I. Vencato, A. J. Bortoluzzi, V. Drago, T. Weyhermuller and E. Rentschler, *Chem. Lett.*, 2000, 540–541.
67 E. Kinoshita, M. Takahashi, H. Takeda, M. Shiro and T. Koike, *Dalton Trans.*, 2004, 1189–1193.
68 L. J. Daumann, K. E. Dalle, G. Schenk, R. P. McGeary, P. V. Bernhardt, D. L. Ollis and L. R. Gahan, *Dalton Trans.*, 2012, **41**, 1695–1708.
69 L. J. Daumann, P. Comba, J. A. Larrabee, G. Schenk, R. Stranger, G. Cavigliasso and L. R. Gahan, *Inorg. Chem.*, 2013, **52**, 2029–2043.
70 J. N. Van Niekerk, F. R. L. Schoening and J. H. Talbot, *Acta Crystallogr.*, 1953, **6**, 720–723.
71 H. Adams, D. Bradshaw and D. E. Fenton, *J. Chem. Soc., Dalton Trans.*, 2002, 925–930.

72 C. Fernandes, A. Neves, A. J. Bortoluzzi, A. S. Mangrich, E. Rentschler, B. Szpoganicz and E. Schwingel, *Inorg. Chim. Acta*, 2001, **320**, 12–21.
73 C. Fernandes, A. J. Bortoluzzi, B. Szpoganicz, E. Schwingel and A. Neves, *Inorg. Chim. Acta*, 2005, **358**, 997–1004.
74 C. Fernandes, A. Neves, A. J. Bortoluzzi, B. Szpoganicz and E. Schwingel, *Inorg. Chem. Commun.*, 2001, **4**, 354–357.
75 A. W. Addison, T. N. Rao, J. Reedijk, J. van Rijn and G. C. Verschoor, *J. Chem. Soc., Dalton Trans.*, 1984, 1349–1356.
76 M. Lanznaster, A. Neves, A. J. Bortoluzzi, V. V. E. Aires, B. Szpoganicz, H. Terenz, P. C. Severino, J. M. Fuller, S. Drew, L. R. Gahan, G. R. Hanson, M. J. Riley and G. Schenk, *J. Biol. Inorg. Chem.*, 2005, **10**, 319–332.
77 T. M. Kitson, *Biochim. Biophys. Acta, Protein Struct. Mol. Enzymol.*, 1998, **1385**, 43–52.
78 T. W. Elliott, N. Mitić, L. R. Gahan, L. W. Guddat and G. Schenk, *J. Braz. Chem. Soc.*, 2006, **17**, 1558–1565.
79 A. Kantacha, R. Buchholz, S. J. Smith, G. Schenk and L. R. Gahan, *J. Biol. Inorg. Chem.*, 2011, **16**, 25–32.
80 Y. L. M. Zee, L. R. Gahan and G. Schenk, *Aust. J. Chem.*, 2011, **64**, 258–264.
81 K. E. Dalle, L. J. Daumann, G. Schenk, R. P. McGeary, L. R. Hanton and L. R. Gahan, *Polyhedron*, 2013, **52**, 1336–1343.
82 R. S. Cox, G. Schenk, N. Mitić, L. R. Gahan and A. C. Hengge, *J. Am. Chem. Soc.*, 2007, **129**, 9550–9551.
83 K. S. Hadler, L. R. Gahan, D. L. Ollis and G. Schenk, *J. Inorg. Biochem.*, 2010, **104**, 211–213.
84 D. G. Gorenstein, *Phosphorus-31 NMR: Principles and Applications*, Academic Press, 1984.
85 X. Liu, P. Du and R. Cao, *Nat. Commun.*, 2013, **4**, 2375.
86 F. Ely, K. S. Hadler, L. R. Gahan, L. W. Guddat, D. L. Ollis and G. Schenk, *Biochem. J.*, 2010, **432**, 565–573.
87 N. Mitic, C. J. Noble, L. R. Gahan, G. R. Hanson and G. Schenk, *J. Am. Chem. Soc.*, 2009, **131**, 8173–8179.
88 N. Mitić, M. Valizadeh, E. W. W. Leung, J. de Jersey, S. Hamilton, D. A. Hume, A. I. Cassady and G. Schenk, *Arch. Biochem. Biophys.*, 2005, **439**, 154–164.
89 A. Neves, M. Lanznaster, A. J. Bortoluzzi, R. A. Peralta, A. Casellato, E. E. Castellano, P. Herrald, M. J. Riley and G. Schenk, *J. Am. Chem. Soc.*, 2007, **129**, 7486–7487.
90 S. J. Smith, A. Casellato, K. S. Hadler, N. Mitic, M. J. Riley, A. J. Bortoluzzi, B. Szpoganicz, G. Schenk, A. Neves and L. R. Gahan, *J. Biol. Inorg. Chem.*, 2007, **12**, 1207–1220.